Reactions of Manganese Silyl Dihydride Complexes with CO_2[†]

Jeffrey S. Price and David J. H. Emslie*

Department of Chemistry, McMaster University, 1280 Main Street West, Hamilton, ON, L8S 4M1, Canada

Supporting Information Placeholder

Abstract

Under mild conditions (room temperature, 1.1 atm. of CO_2), the silyl dihydride complexes $[(dmpe)_2MnH_2(SiHR_2)]$ {R = Ph (**1**^{Ph2}); Et (**1**^{Et2})} reacted rapidly and quantitatively with carbon dioxide to afford $[(dmpe)_2MnH_2\{Si(\kappa^1\text{-}O_2CH)R_2)\}]$ {R = Ph (**2**^{Ph2}); Et (**2**^{Et2})}; the products of apparent CO_2 insertion into the terminal Si–H bond. In addition, room temperature reactions of $[(dmpe)_2MnH_2(SiH_2R)]$ {R = Ph (**1**^{Ph}); ^{n}Bu (**1**^{Bu})} with CO_2 (1.1 atm.) yielded $[(dmpe)_2MnH_2\{Si(\kappa^1\text{-}O_2CH)_2R)\}]$ {R = Ph (**3**^{Ph}); ^{n}Bu (**3**^{Bu})} containing two formate substituents on silicon. The latter reactions proceeded in a stepwise fashion, rapidly forming $[(dmpe)_2MnH_2\{SiH(\kappa^1\text{-}O_2CH)R\}]$ {R = Ph (**4**^{Ph}); ^{n}Bu (**4**^{Bu})} intermediates, which then slowly converted into **3**^{Ph} and **3**^{Bu}. During the syntheses of **3**^{Ph} and **3**^{Bu}, significant amounts of H_2 and previously reported $[(dmpe)_2Mn(CO)(\kappa^1\text{-}O_2CH)]$ (**5**) were also formed. The reaction of $[(dmpe)_2MnD_2(SiH_2{}^n\text{Bu})]$ (***d*$_2$-1**^{Bu}) with CO_2 was carried out, yielding ***d*$_2$-3**^{Bu} as the major reaction product, predominantly (>95%) as $[(dmpe)_2MnD_2\{Si(\kappa^1\text{-}O_2CH)_2{}^n\text{Bu}\}]$ featuring two deuteride ligands. DFT calculations to probe the relative energies of silicate $[(dmpe)_2Mn(\eta^3\text{-}H_2SiR_3)]$, *trans*-hydrosilane/hydride (*trans*-$[(dmpe)_2MnH(H\text{–}SiR_3)]$), *trans*-dihydrogen/silyl (*trans*-$[(dmpe)_2Mn(H_2)(SiR_3)]$), and *lateral*-dihydrogen/silyl (*cis*-$[(dmpe)_2Mn(H_2)(SiR_3)]$) isomers of **2**^{Ph2}, **3**^{Ph}, and **4**^{Ph} are also reported; the lowest energy structures of **2**^{Ph2} and **3**^{Ph} are those of the silicate isomers, consistent with the NMR spectra obtained for **2**^{R2} and **3**^{R}. Also, compound **2**^{Ph2} was isolated, and crystallized as the silicate isomer; the solid state structure of **2**^{Ph2} is qualitatively analogous to that of **1**^{Ph2}, but the Mn–Si bond in **2**^{Ph2} is significantly shorter {2.2876(7) Å vs 2.3176(3) Å}.

[†] Part of the special issue dedicated to the element manganese, entitled "Manganese: A Tribute to Chemical Diversity".

Introduction

Insertion of unsaturated organic reagents into an Si–H bond (hydrosilylation) is an important process to incorporate silicon into higher value products.[1] Hydrosilylation of carbon dioxide is of particular interest, given that CO_2 is a widely available and inexpensive C1 synthon.[2] However, despite the considerable thermodynamic driving force for CO_2 insertion into an Si–H bond to generate an Si–O bond (Si–O BDE = 798(8) kJ mol^{-1}),[3] this reaction is kinetically disfavoured for most free hydrosilanes. These insertion reactions can be catalyzed by transition metals,[1,2] and are most commonly reported to follow cycles akin to the Chalk-Harrod[4] and modified Chalk-Harrod[5] cycles for olefin hydrosilylation (or the closely related Ojima cycle[6] for hydrosilylation of carbonyl compounds). In these cycles, key steps are hydrosilane Si–H bond oxidative addition, coordination of the unsaturated substrate to the metal center, insertion into a metal–hydride or metal–silyl linkage, and reductive elimination to release the hydrosilylated product.

An alternative catalytic cycle for ketone hydrosilylation was proposed in 1995 by Zheng and Chan, involving direct ketone insertion into the terminal Si–H bond of a rhodium silyl complex.[7] However, strong evidence for this mechanism has not been presented.[8, 9] Recently, the Tilley group developed a new catalytic hydrosilylation route predicated on direct insertion of the unsaturated organic reagent into an 'activated' Si–H bond; the Glaser-Tilley mechanism for olefin hydrosilylation, which involves alkene insertion into the terminal Si–H bond of a transition metal silylene complex (Figure 1; left).[10] Similar catalytic chemistry based on alkene or alkyne insertion into an Si–H bond has been reported for silylene-like transition metal η^3-H_2SiRH complexes.[11] In addition, the Tobita group reported the overall insertion of acetone into the terminal Si–H bond of a tungsten silylene complex containing a hydride co-ligand, though a Glaser-Tilley-like mechanism (involving direct insertion of the C=O bond into a terminal silylene Si–H bond) was computationally determined to be higher in energy than alternative mechanisms.[12] Furthermore, the Tilley group reported overall insertion of aldehydes and ketones into the terminal Si–H bond in silylene iridium cations, though it is unclear if this reaction proceeds via (Glaser-Tilley-like) direct insertion or an alternative mechanism.[13] More recently, Tilley and Lipke have demonstrated that η^3-H_2SiRH complexes with a hydride co-ligand are active catalysts for ketone hydrosilylation, and proposed a mechanism involving initial formation of an $L_xRu(\mu\text{-}H)_3SiR_2(O{=}CR'_2)$ species by coordination of both a hydride co-ligand and the ketone to silicon, followed by insertion of the C=O bond into one of the Si–(μ-H) bonds (Figure 1; right).[9] The classes of transition metal complexes which have been shown to undergo direct CO_2 insertion into an Si–H bond are notable in that the Si centers are significantly more electrophilic than those in free hydrosilanes or transition metal silyl complexes; the utility of electrophilic Si–H bond activation (which refers to Si–H bond activation as a consequence of substantial electrophilicity at silicon) is a subject of significant investigation.[8]

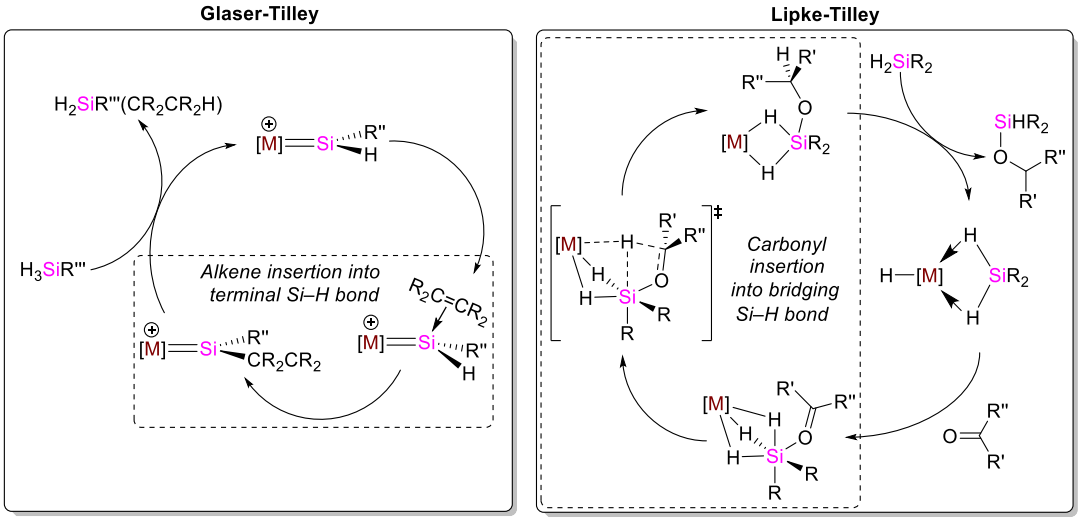

Figure 1. Glaser-Tilley and Lipke-Tilley hydrosilylation mechanisms.

Over the past few decades, it has also been demonstrated that the Si–H bond is activated towards carbonyl insertion chemistry in metal-free hypercoordinate silicon species, which feature increased Lewis acidity of the Si centers and enhanced hydridic character of the Si*H* substituents relative to ubiquitous 4-coordinate hydrosilanes.[14] For example, 5-coordinate metal-free amine-substituted hydrosilanes (a in Figure 2) have been reported to undergo room-temperature insertion of a C=O bond (from an aldehyde, ketone, or carbon dioxide) into the Si–H bond.[15] A 4-coordinate hydrosilane with a guanidinyl substituent (b in Figure 2) has also been demonstrated to undergo similar reactivity, and DFT calculations suggested that the pendent Lewis base coordinates to silicon to form an unobserved hypercoordinate intermediate prior to CO_2 activation.[16] Furthermore, a stable 6-coordinate silicon dihydride species stabilized by a tetradentate porphyrin ligand (c in Figure 2) was shown to undergo C=O insertion reactivity upon exposure to aldehydes or carbon dioxide under mild conditions {in this case, given that silicon is already 6-coordinate, CO_2 insertion was proposed to occur via hydride abstraction from silicon (by CO_2) to generate a free formate anion and a 5-coordinate silyl cation, followed by formate coordination to silicon}.[17] Insertion reactions of other unsaturated organic reagents such as isocyanates,[18] isothiocyanates,[18] and imines[19] into the Si–H bonds in hypercoordinate amine-substituted hydrosilanes have also been reported. It is notable that the proposed reactive intermediate in the Lipke-Tilley cycle for catalytic ketone hydrosilylation (Figure 1; right) features a hypercoordinate Si center with (in addition to the ketone donor) two terminal substituents on Si and three hydrides bridging between Si and the metal center.[9]

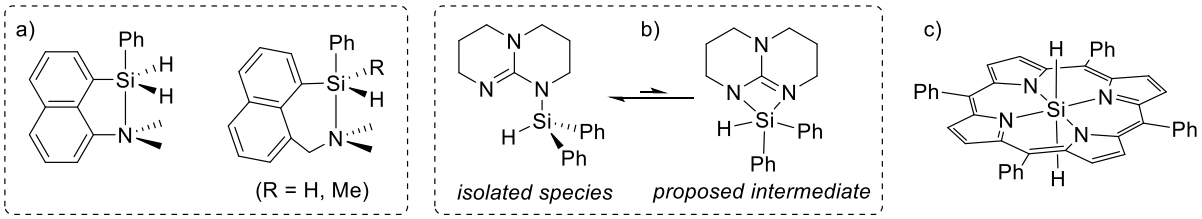

Figure 2. Metal-free hypercoordinate Si species for which carbonyl insertion into an Si–H bond has been reported: a) 5-coordinate amine-substituted hydrosilanes,[15] b) a 4-coordinate hydrosilane which

undergoes CO_2 insertion via a 5-coordinate intermediate,[16] and c) a 6-coordinate porphyrin silicon dihydride.[17]

Another class of stable Si-containing species where the silicon is hypercoordinate are transition metal silicate complexes, where two hydride ligands bridge between the metal and an SiR_3 unit. Therefore, if one of the terminal substituents on silicon is a hydride, it would be of interest to determine if insertion of unsaturated organic reagents into the terminal Si–H bond would occur. The first transition metal silicate complex, $[(Me_2PhP)_3Re(CO)(\eta^3\text{-}H_2SiPh_3)]$, was reported by the Crabtree group in 1990, though the bridging hydride atoms were not crystallographically located.[20] Since that time, approximately a dozen crystallographically authenticated monometallic transition metal silicate-like complexes have been reported for Cr,[21] Mo,[22] Mn,[23, 24] Fe,[25] Ru,[26] Co,[27] and Rh.[28] Of these, it is notable that $[(^iPr_2MeP)CpFe(\eta^3\text{-}H_2SiHMePh)]$ demonstrated some activity towards catalytic hydrosilylation of benzaldehyde by H_3SiPh, though the cationic silicate-free analogue $[(^iPr_2MeP)CpFe(NCCH_3)_2]^+$ showed higher activity.[25] Furthermore, a catalytic cycle for alkene hydrosilylation has recently been proposed (based on deuterium labelling and kinetic studies) involving alkene insertion into the terminal Si–H bond of a putative nickel silicate intermediate.[29] Our group reported the manganese 'silyl dihydride' complexes (**1**), which exist in solution as a mixture of a silicate ($[(dmpe)_2Mn(\eta^3\text{-}H_2SiHRR')]$) and a *trans*-hydrosilane/hydride (*trans*-$[(dmpe)_2MnH(H–SiHRR')]$) isomer; Figure 3. DFT calculations further suggested the thermodynamic accessibility of two more isomers; *trans*- and *lateral*- dihydrogen/silyl species (Figure 3; these isomers were 8−44 kJ mol^{-1} higher in energy than the most stable experimentally observed isomer, depending on the substitution pattern; for clarity, the silyl dihydride formalism and the chemical formula $[(dmpe)_2MnH_2(SiR_3)]$ will herein refer to all isomers).[24] At elevated temperature, these species were active for ethylene hydrosilylation catalysis. However it was proposed that this chemistry proceeds via H_2 elimination to form a catalytically active manganese silylene hydride or low-coordinate silyl species.[30] Herein, we discuss the reactions of manganese silyl dihydride complexes, **1**, with carbon dioxide.

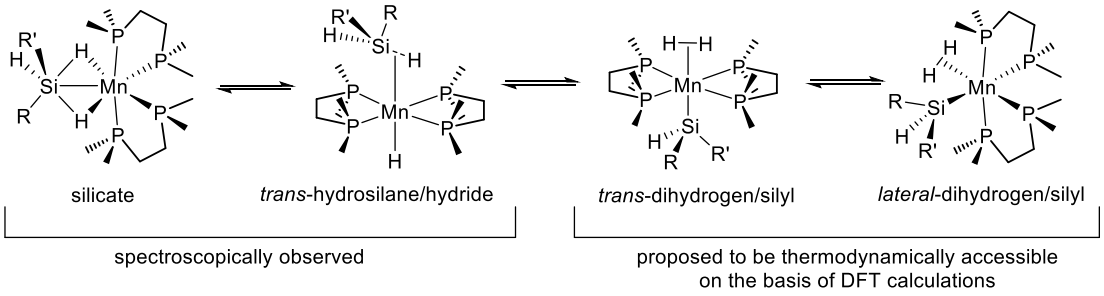

Figure 3. Isomers of silyl dihydride complexes $[(dmpe)_2MnH_2(SiHRR')]$ {R = R' = Ph (**1**^{Ph2}); R = R' = Et (**1**^{Et2}); R = Ph, R' = H (**1**^{Ph}); R = ^{n}Bu, R' = H (**1**^{Bu})} proposed to be accessible in solution.[24]

Results and Discussion

Synthesis and Characterization: The manganese silyl dihydride complexes [(dmpe)$_2$MnH$_2$(SiHR$_2$)] {R = Ph (**1**^{Ph2}); Et (**1**^{Et2})} (which exist in solution as an equilibrium between silicate and hydrosilane/hydride isomers; *vide supra*) reacted with CO_2 (1.1 atm.) to afford [(dmpe)$_2$MnH$_2${Si(κ^1-O$_2$CH)R$_2$)}] {R = Ph (**2**^{Ph2}); Et (**2**^{Et2})}, in which the H substituent on silicon has been converted to a formate group (Scheme 1). These reactions reached completion within minutes at room temperature, with quantitative formation of **2**^{Ph2} and **2**^{Et2} by NMR spectroscopy; **2**^{Ph2} was isolated in 66% yield.

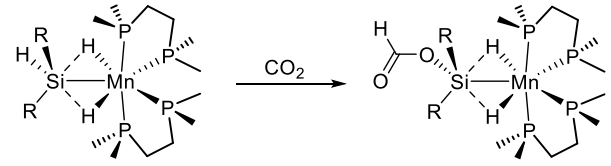

R = Ph (**1**^{Ph2}) or Et (**1**^{Et2}) R = Ph (**2**^{Ph2}) or Et (**2**^{Et2})

Scheme 1. Reactions of silyl dihydride complexes [(dmpe)$_2$MnH$_2$(SiHR$_2$)] {R = Ph (**1**^{Ph2}); Et (**1**^{Et2})} with CO_2 to yield [(dmpe)$_2$MnH$_2${Si(κ^1-O$_2$CH)R$_2$)}] {R = Ph (**2**^{Ph2}); Et (**2**^{Et2})}. Only one isomer of **1**^{Ph2} and **1**^{Et2} is shown.

Solution ^{1}H and ^{13}C{^{1}H} NMR spectra of **2**^{Ph2} and **2**^{Et2} in d_8-toluene or C_6D_6 feature a single set of peaks, including a Mn*H* signal at –13.5 or –13.8 ppm, respectively, an O$_2$C*H* peak at 8.7-8.9 ppm, and two sets of signals for the diastereotopic phenyl or ethyl groups. These data (see Table 1 for selected data), along with observation of two broad ^{31}P NMR resonances at approximately 70 ppm, are consistent with that obtained for the silicate isomer of formate-free silyl dihydride analogues **1**. The observation of just one MnH signal and two ^{31}P signals is indicative of fluxional solution behaviour, possibly involving a flip in the butterfly Mn(μ-H)$_2$Si core of the molecule and 180° rotation about the Mn–Si bond, as illustrated in Figure 4 (an equilibrium with a *trans*-hydrosilane hydride isomer would not explain the observed NMR spectra given that this would render all four phosphorus donors and both R substituents of the SiR$_2$(O$_2$CH) group equivalent). ^{29}Si NMR resonances were observed at 39.3 and 53.9 ppm, which are shifted to high frequency relative to the silicate isomers of **1**^{Ph2} and **1**^{Et2} (10.0 and 14.2 ppm). In d_8-toluene, **2**^{Ph2} gave rise to signals attributable to a single silicate isomer down to 190 K. This contrasts the behaviour of **1**^{Ph2} and **1**^{Et2} which exist as a mixture of the silicate and *trans*-hydrosilane/hydride isomers in a 6.7:1 or 3.5:1 ratio (at 298 K), respectively.[23]

Table 1. Selected NMR Chemical Shifts (ppm) for the Silicate Isomers of Silyl Dihydride Complexes [(dmpe)$_2$MnH$_2$(SiHR$_2$)] {R = Ph (**1**^{Ph2}); Et (**1**^{Et2})},[23] [(dmpe)$_2$MnH$_2$(SiH$_2$R)] {R = Ph (**1**^{Ph}); ^{n}Bu (**1**^{Bu})},[24] [(dmpe)$_2$MnH$_2${Si(κ^1-O$_2$CH)R$_2$)}] {R = Ph (**2**^{Ph2}); Et (**2**^{Et2})}, [(dmpe)$_2$MnH$_2${Si(κ^1-O$_2$CH)$_2$R)}] {R = Ph (**3**^{Ph}); ^{n}Bu (**3**^{Bu})}, and [(dmpe)$_2$MnH$_2${{SiH(κ^1-O$_2$CH)R)}] {R = Ph (**4**^{Ph}); ^{n}Bu (**4**^{Bu})}. Unless otherwise indicated, spectra were obtained in C_6D_6 at room temperature (500 or 600 MHz). n.l. indicates that an environment was not located.

	silyl group[(a)]	^{1}H			^{13}C	^{29}Si	^{31}P
		(Mn*H*)	(κ^1-O$_2$CH)	(Si*H*)	(κ^1-O$_2$*C*H)		
1^{Ph2}[(b)]	SiHPh$_2$	–12.5	–	6.6	–	10.0	71.0, 72.2
1^{Et2}[(b)]	SiHEt$_2$	–12.7	–	5.0	–	14.2	71.7, 75.2
1^{Ph}[(b)]	SiH$_2$Ph	–12.8	–	6.0, 6.1	–	–15.7	72.4, 74.0

1^{Bu}(*b*)	$SiH_2{}^nBu$	–12.8	–	5.2, 5.4	–	–22.0	72.1, 74.1
2^{Ph2}(*c*)	$Si(\kappa^1\text{-}O_2CH)Ph_2$	–13.5	8.9	–	162.6	39.3	68.7, 69.6
2^{Et2}	$Si(\kappa^1\text{-}O_2CH)Et_2$	–13.8	8.7	–	162.5	53.9	69.1, 72.0
3^{Ph}	$Si(\kappa^1\text{-}O_2CH)_2Ph$	–13.9	8.5, 8.8	–	161.0, 161.8	34.2	68.2, 71.1
3^{Bu}	$Si(\kappa^1\text{-}O_2CH)_2{}^nBu$	–14.0	8.6, 8.6	–	160.9, 161.5	46.5	67.9, 72.5
4^{Ph}(*d*)	$SiH(\kappa^1\text{-}O_2CH)Ph$	–13.5	8.8	6.9	n.l.	31.3	69.4, 72.1
4^{Bu}(*d*)	$SiH(\kappa^1\text{-}O_2CH){}^nBu$	–13.7	8.7	6.3	n.l.	n.l.	n.l.

a. Not including hydrides interacting with the metal centre.

b. Spectra were obtained in d_8-toluene at various temperatures due to the need to resolve the silicate isomer from additional isomers in solution (values from References 23 and 24).

c. Spectra were obtained in d_8-toluene due to poor solubility in C_6D_6.

d. For intermediates **4**^{Ph} and **4**^{Bu}, it is unclear whether the NMR data corresponds to the silicate isomer or to an average of multiple isomers in rapid equilibrium.

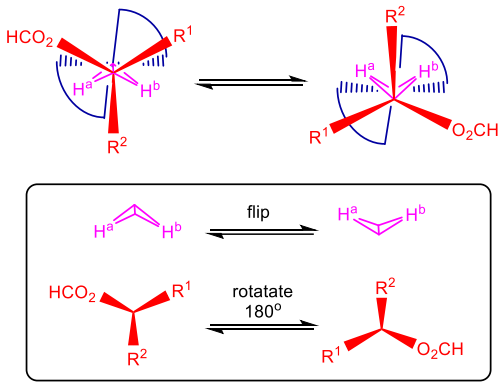

Figure 4. A potential fluxional process to explain the observation of a single MnH ^{1}H NMR signal and just two ^{31}P NMR signals for **2**^{Ph2} and **2**^{Et2}. For clarity, Mn, P, and Si atoms are not labelled. The "Mn(dmpe)$_2$" fragment is shown in blue. The "$SiR_2(O_2CH)$" fragment is shown in red. The butterfly Mn(μ-H)$_2$Si core of the molecule is shown in pink. R^1 and R^2 are the diastereotopic phenyl or ethyl groups in **2**^{Ph2} and **2**^{Et2}, respectively. H^a and H^b are the two MnH environments that are rendered equivalent through the proposed fluxional process. This fluxional process involves a flip in the butterfly Mn(μ-H)$_2$Si core of the molecule and 180° rotation about the Mn–Si bond, as illustrated in the box.

X-ray quality crystals of **2**^{Ph2} were obtained by layering a THF solution of **2**^{Ph2} with hexanes and cooling to –30 °C. Compound **2**^{Ph2} crystallized as the expected silicate isomer (A in Figure 5), in which the five organic substituents on silicon form an approximate square pyramid, with one of the two phenyl rings in the apical site (substituents in the square plane are the two hydride ligands, the formate group, and the second phenyl ring). The structure of **2**^{Ph2} is qualitatively isostructural with that of **1**^{Ph2} (B in Figure 5),[23] with the position occupied by the terminal Si*H* substituent now occupied by the formate group. However, relative to the isostructural formate-free precursor **1**^{Ph2},[23] the Mn–Si distance in **2**^{Ph2} is significantly shorter {2.2876(7) Å vs. 2.3176(3) Å}, despite the increased steric congestion around silicon. This may be due to increased backdonation from Mn to the silicate ligand, given that the Hirshfeld charge on silicon becomes more positive upon replacement of an H substituent with a formate substituent (e.g. 0.210[24] in **1**^{Ph2} vs 0.285 in **2**^{Ph2} or 0.180[24] in **1**^{Ph} vs 0.256 in **4**^{Ph} vs 0.316 in **3**^{Ph}).

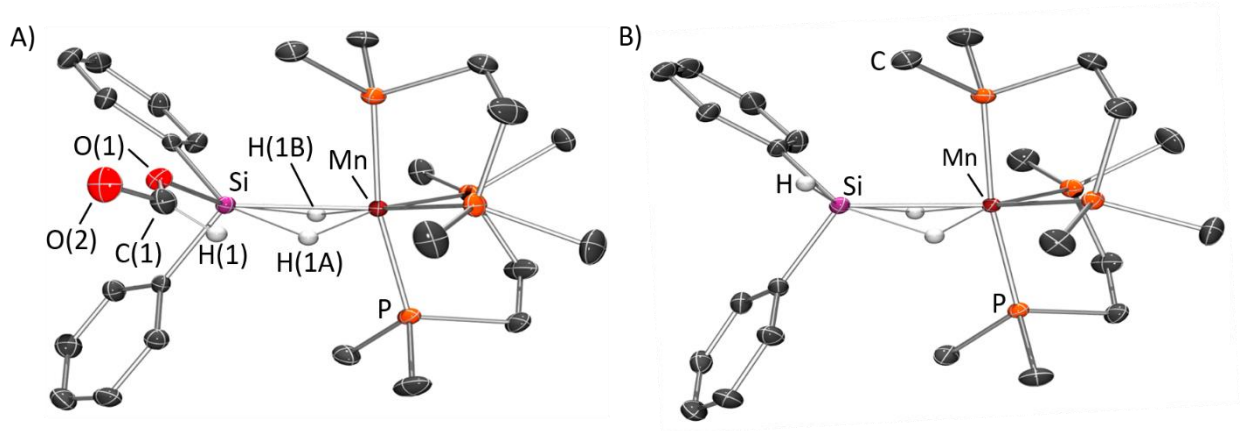

Figure 5. A) X-ray crystal structure of [(dmpe)$_2$MnH$_2${Si(κ^1-O$_2$CH)Ph$_2$}] (**2^{Ph2}**) with ellipsoids drawn at 50% probability. The two metal hydride atoms and the hydrogen atom on the formate substituent were located from the difference map and refined isotropically. All other hydrogen atoms have been omitted for clarity. Bond distances (Å) and angles (deg): Mn–Si 2.2876(7), Mn–H(1A) 1.52(3), Mn–H(1B) 1.55(3), Si–H(1A) 1.79(3), Si–H(1B) 1.75(3), Si–O(1) 1.783(2), O(1)–C(1) 1.305(3), C(1)–O(2) 1.212(3), C(1)–H(1) 0.97(3), H(1A)–Mn–H(1B) 94(2), H(1A)–Si–H(1B) 78(1), H(1A)–Mn–Si 51(1), H(1B)–Mn–Si 50(1), Mn–Si–C(2) 120.08(7), Mn–Si–C(8) 119.48(7), Mn–Si–O(1) 119.46(6), Si–O(1)–C(1) 128.3(2), O(1)–C(1)–O(2) 124.4(2), O(1)–C(1)–H(1) 117(2), plane{H(1A)–Mn–H(1B)}/plane{H(1A)–Si–H(1B)} 38.1. B) The previously reported X-ray crystal structure of [(dmpe)$_2$MnH$_2$(SiHPh$_2$)] (**1^{Ph2}**)[23] is shown for comparison.

Reactions of CO_2 (1.1 atm.) with [(dmpe)$_2$MnH$_2$(SiH$_2$R)] {R = Ph (**1^{Ph}**); ^{n}Bu (**1^{Bu}**)}, containing two Si*H* substituents, were also explored. These reactions (Scheme 2) proceeded in a stepwise fashion, initially forming [(dmpe)$_2$MnH$_2${SiH(κ^1-O$_2$CH)R}] {R = Ph (**4^{Ph}**); ^{n}Bu (**4^{Bu}**)} intermediates, which then converted into [(dmpe)$_2$MnH$_2${Si(κ^1-O$_2$CH)$_2$R)}] {R = Ph (**3^{Ph}**); ^{n}Bu (**3^{Bu}**)}. The first step (to form **4^{Ph}** and **4^{Bu}**) was complete within minutes at room temperature, whereas the second step (to form **3^{Ph}** and **3^{Bu}**) was much slower; an approximate 1 : 4 ratio of **4^{Ph}** : **3^{Ph}** was observed after 5 days (Figure 6), and complete consumption of **4^{Bu}** was observed after 2 days. During the course of these reactions, significant amounts of H_2 and previously reported [(dmpe)$_2$Mn(CO)(κ^1-O$_2$CH)] (**5**) were also formed; an approximate 1 : 0.4 ratio of **3^{Ph}** : **5** or **3^{Bu}** : **5** was observed after two (for **3^{Ph}**) or one (for **3^{Bu}**) week(s). Compound **5** could potentially be formed via H_2 elimination from **4^{R}** or **3^{R}** to form a 5-coordinate silyl complex, [(dmpe)$_2$Mn{SiX(κ^1-O$_2$CH)R}] (X = H or κ^1-O$_2$CH), and we have previously proposed intermediates of this type in the synthesis of **5** from disilylhydride complexes ([(dmpe)$_2$MnH(SiH$_2$R)$_2$]; R = Ph or ^{n}Bu) and CO_2.[31] Indeed, upon completion of the reaction, some conversion of **3^{Ph}** and **3^{Bu}** into **5** was observed over the course of several days. By contrast, **5** was not observed in reactions of **1^{Ph2}** or **1^{Et2}** with CO_2, and no room temperature decomposition was observed for **2^{Ph2}** in C_6D_6 under a CO_2 atmosphere over 5 days.

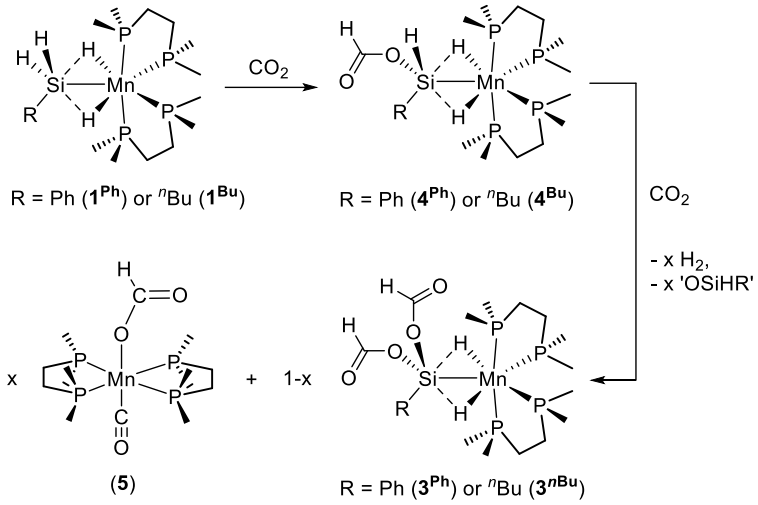

Scheme 2. Reactions of [(dmpe)$_2$MnH$_2$(SiH$_2$R)] {R = Ph (**1**^{Ph}); ^{n}Bu (**1**^{Bu})} with CO_2, resulting in initial formation of [(dmpe)$_2$MnH$_2${SiH(κ^1-O$_2$CH)R}] {R = Ph (**4**^{Ph}); ^{n}Bu (**4**^{Bu})}, followed by conversion to a mixture of [(dmpe)$_2$MnH$_2${Si(κ^1-O$_2$CH)$_2$R)}] {R = Ph (**3**^{Ph}); ^{n}Bu (**3**^{Bu})} and [(dmpe)$_2$Mn(CO)(κ^1-O$_2$CH)] (**5**). H_2 was detected as a byproduct associated with the formation of **5**, and 'OSiHR' is hypothesized (based on the reaction stoichiometry and related work[31]) but was not detected. Compounds **3**^{Ph} and **3**^{Bu} slowly converted to **5** at room temperature (not shown).

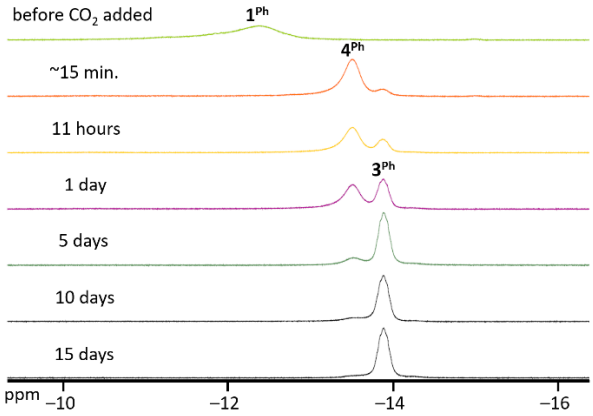

Figure 6. The metal hydride region of ^{1}H NMR spectra for the reaction of [(dmpe)$_2$MnH$_2$(SiH$_2$Ph)] (**1**^{Ph}) with CO_2. The initially formed hydride product is assigned as [(dmpe)$_2$MnH$_2${SiH(κ^1-O$_2$CH)Ph}] (**4**^{Ph}), which slowly reacted with a 2nd equivalent of CO_2 to afford [(dmpe)$_2$MnH$_2${Si(κ^1-O$_2$CH)$_2$Ph)}] (**3**^{Ph}).

NMR spectra for **3**^{Ph} and **3**^{Bu} are very similar to those of **2**^{Ph2} and **2**^{Et2} (see Table 1 for data), but with two inequivalent formate groups and one hydrocarbyl group on silicon, and ^{29}Si resonances at slightly lower frequency (34.2 and 46.5 ppm, respectively). Spectroscopic analysis of intermediates **4**^{Ph} and **4**^{Bu} was more limited, given that samples of these compounds always contained some **3**^{Ph} and **3**^{Bu}. Nevertheless, Mn*H*, Si*H* and O$_2$C*H* signals were clearly identified in the ^{1}H NMR spectrum, with integrations of 2H, 1H and 1H, respectively.

DFT Calculations on Products and Intermediates: Only one isomer (silicate) was observed spectroscopically for formate-substituted silyl dihydride complexes **2**^{Ph2}, **2**^{Et2}, **3**^{Ph} and **3**^{Bu} (and crystallographically for **2**^{Ph2}). By contrast, two isomers (silicate and *trans*-hydrosilane/hydride species) were observed for formate-free **1**^{Ph2}, **1**^{Et2}, **1**^{Ph} and **1**^{Bu}, and DFT calculations indicated the thermodynamic accessibility of two additional isomers (*trans*- and *lateral*-dihydrogen/silyl species); Figure 3.[24] Consequently, DFT calculations (ADF, gas phase, all-electron, PBE, D3-BJ, TZ2P, ZORA) were carried out on [(dmpe)$_2$MnH$_2${Si(κ^1-O$_2$CH)Ph$_2$}] (**2**^{Ph2}), [(dmpe)$_2$MnH$_2${Si(κ^1-O$_2$CH)$_2$Ph}] (**3**^{Ph}), and [(dmpe)$_2$MnH$_2${SiH(κ^1-O$_2$CH)Ph}] (**4**^{Ph}) to determine the relative energies of the aforementioned isomers. For **2**^{Ph2}, **3**^{Ph} and **4**^{Ph}, energy minima were located for silicate, *trans*-hydrosilane/hydride (as described previously, these species can be considered to feature nonclassical hydrosilane ligands; the result of significant but incomplete hydrosilane oxidative addition),[24] *trans*-dihydrogen/silyl, and *lateral*-dihydrogen/silyl isomers {see Figure 7 for the structures of the four isomers of **2**^{Ph2}; equivalent figures for **3**^{Ph} and **4**^{Ph} are located in the supporting information (Figures S1 and S2)}.

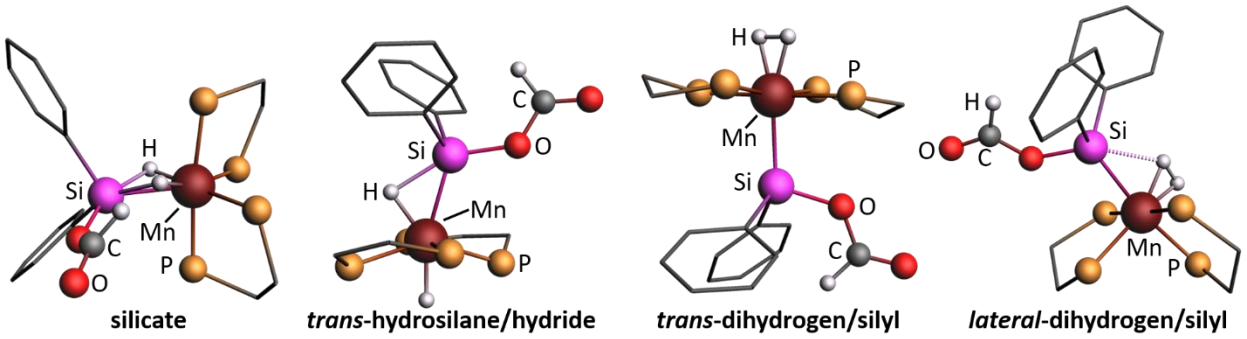

Figure 7. Geometry-optimized structures for isomers of [(dmpe)$_2$MnH$_2${Si(κ^1-O$_2$CH)Ph$_2$}] (**2**^{Ph2}) determined by DFT. Spheres represent Mn (dark red), Si (pink), P (orange), O (bright red), C (grey), and H (white). Most carbon atoms are represented by grey vertices. Methyl groups on dmpe and most H atoms have been omitted for clarity.

The structures of these minima are qualitatively similar to those previously reported[24] for formate-free silyl dihydride complexes **1**^{Ph2} and **1**^{Ph} (selected bond metrics and Mayer bond orders for **2**^{Ph2}, **3**^{Ph}, and **4**^{Ph} are tabulated in the ESI). However, as hydride substituents on silicon are replaced with formate groups, stronger Mn–Si interactions (evident from shorter Mn–Si distances and higher Mayer bond orders) were observed for all four isomers. For compounds with two phenyl groups on silicon, the Mn–Si Mayer bond orders for the silicate, *trans*-hydrosilane/hydride, *trans*-dihydrogen/silyl and *lateral*-dihydrogen/silyl isomers of formate-substituted [(dmpe)$_2$MnH$_2${Si(κ^1-O$_2$CH)Ph$_2$}] (**2**^{Ph2}) are 0.66, 0.89, 0.97 and 0.97, respectively, compared with 0.63, 0.77, 0.95, and 0.91 for formate-free [(dmpe)$_2$MnH$_2$(SiHPh$_2$)] (**1**^{Ph2}). Similarly, the Mayer bond orders for the four isomers of [(dmpe)$_2$MnH$_2${Si(κ^1-O$_2$CH)$_2$Ph)}] (**3**^{Ph}) are 0.76, 0.95, 1.09 and 1.04, respectively, which are greater than those for mono-formate substituted [(dmpe)$_2$MnH$_2${SiH(κ^1-O$_2$CH)Ph)}] (**4**^{Ph}; 0.74, 0.82, 1.01, and 0.97) and formate-free [(dmpe)$_2$MnH$_2$(SiH$_2$Ph)] (**1**^{Ph}; 0.69, 0.81, 0.96, and 0.91).

Relative energies of the silicate, *trans*-hydrosilane/hydride, *trans*-dihydrogen/silyl and *lateral*-dihydrogen/silyl isomers for **2**^{Ph2}, **3**^{Ph} and **4**^{Ph}, as well as formate-free **1**^{Ph2} and **1**^{Ph}, are plotted in Figure 8. For [(dmpe)$_2$MnH$_2${Si(κ^1-O$_2$CH)Ph$_2$}] (**2**^{Ph2}) and [(dmpe)$_2$MnH$_2${Si(κ^1-O$_2$CH)$_2$Ph}] (**3**^{Ph}), which lack Si*H* substituents, the global minimum is the silicate isomer. The *trans*-hydrosilane/hydride isomer is approximately 12 kJ mol^{-1} higher in energy, and the remaining two isomers (*trans*- and *lateral*-

dihydrogen/silyl) are 26-45 kJ mol^{-1} higher in energy. Consistent with these data, only the silicate isomer of **2**^{Ph2} (and **2**^{Et2}) was observed by solution NMR spectroscopy, and in the X-ray crystal structure of **2**^{Ph2}. By contrast, for formate-free [(dmpe)$_2$MnH$_2$(SiHPh$_2$)] (**1**^{Ph2}) and [(dmpe)$_2$MnH$_2$(SiH$_2$Ph)] (**1**^{Ph}), the silicate and *trans*-hydrosilane/hydride isomers were similar in energy, and both were observed in solution NMR studies.[24] Similar to **1**^{Ph2} and **1**^{Ph}, the silicate and *trans*-hydrosilane/hydride isomers of [(dmpe)$_2$MnH$_2${SiH(κ^1-O$_2$CH)Ph}] (**4**^{Ph}) are comparable in energy (within 3 kJ mol^{-1}), suggesting that both isomers of **4**^{Ph} (which was not fully spectroscopically characterized due to insertion of a second equivalent of CO$_2$) may be present in solution.

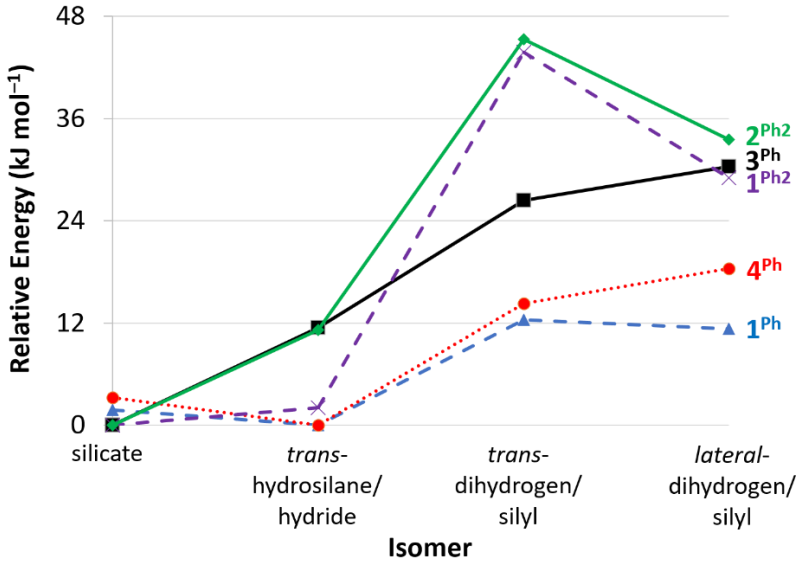

Figure 8. Relative total bonding energies (kJ mol^{-1}) of the silicate, *trans*-hydrosilane/hydride, *trans*-dihydrogen/silyl, and *lateral*-dihydrogen/silyl isomers of silyl dihydride complexes: [(dmpe)$_2$MnH$_2${Si(κ^1-O$_2$CH)Ph$_2$}] (**2**^{Ph2}; green solid line and diamonds), [(dmpe)$_2$MnH$_2${Si(κ^1-O$_2$CH)$_2$Ph}] (**3**^{Ph}; black solid line and squares), and [(dmpe)$_2$MnH$_2${SiH(κ^1-O$_2$CH)Ph}] (**4**^{Ph}; red dotted line and circles), as well as previously reported formate-free analogues [(dmpe)$_2$MnH$_2$(SiHPh$_2$)] (**1**^{Ph2}; purple dashed line and crosses) and [(dmpe)$_2$MnH$_2$(SiH$_2$Ph)] (**1**^{Ph}; blue dashed line and triangles).[24]

Deuterium Labelling and Mechanistic Notes: Reaction of [(dmpe)$_2$MnD$_2$(SiH$_2$^{n}Bu)] (***d*$_2$-1**^{Bu}) with CO$_2$ formed ***d*$_2$-3**^{Bu} as the major reaction product, and based on integration of the hydride and formate signals in the ^{1}H NMR spectrum, this product is predominantly (>95%) [(dmpe)$_2$MnD$_2${Si(κ^1-O$_2$CH)$_2$^{n}Bu}] featuring two deuteride ligands. This labelling experiment is consistent with a mechanism involving direct insertion of CO$_2$ into a terminal Si–H bond (pathway i in Scheme 3) of the silicate isomer[32] of ***d*$_2$-1**^{Bu} (or, for the second insertion, ***d*$_2$-4**^{Bu}),[33] and similar direct CO$_2$ insertion reactivity has been proposed for other hypercoordinate silicon species as discussed in the introduction. However, metal-based mechanisms that are consistent with the deuterium labelling experiment can also be envisaged. These mechanisms presumably require initial generation of a vacant coordination site to allow CO$_2$ binding to manganese, either via dihydrogen dissociation (from a dihydrogen silyl isomer) or phosphine dissociation. However, complete conversion of **1**^{R2} to **2**^{R2} occurred in minutes at room temperature (under 1.1 atm. of CO$_2$), which suggests that initial H$_2$ (or HSiR$_3$) elimination from **1**^{R2}, which we have previously shown is not rapid at room temperature,[24] is unlikely to be involved. Consequently, the more plausible metal-based pathway

is: (i) phosphine dissociation to generate a vacant coordination site, (ii) coordination of CO_2 to manganese and insertion into the Mn–Si bond, generating a Mn–C(O)OSiHRR' linkage,[34] (iii) conversion to a Mn–Si(O_2CH)RR' isomer via Si–H bond oxidative addition followed by C–H bond-forming reductive elimination (or σ-bond metathesis), and (iv) phosphine re-coordination (pathway ii in Scheme 3).

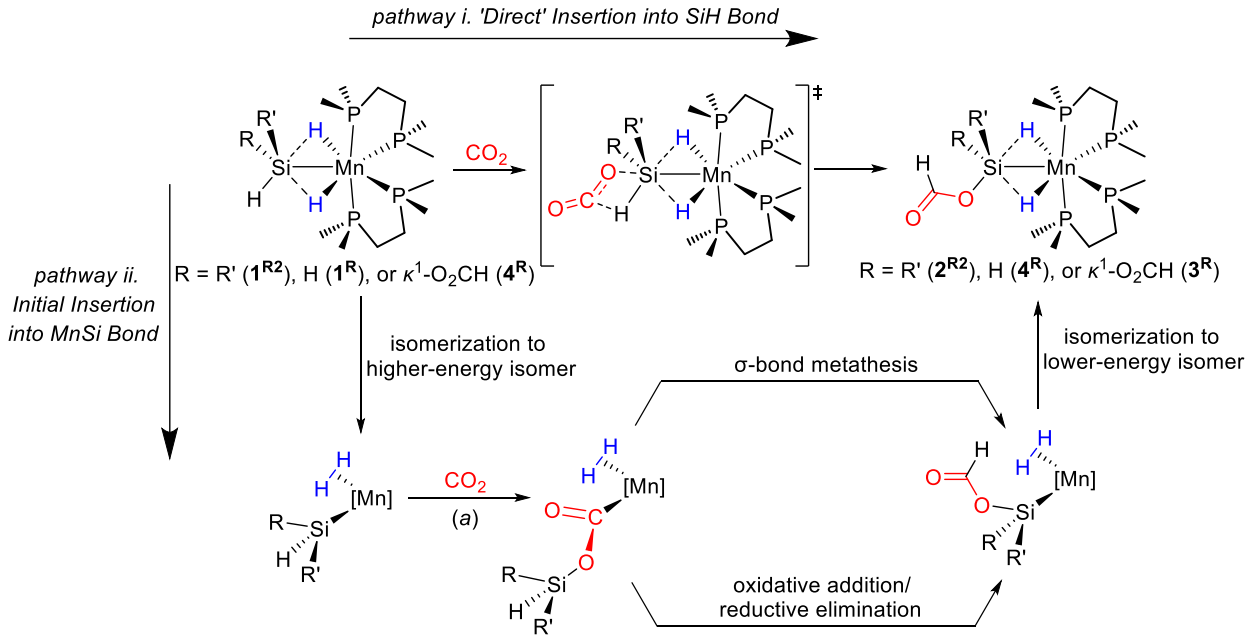

Scheme 3. Potential pathways for CO_2 insertion into silyl dihydride complexes with terminal Si*H* substituents (**1** and **4**) consistent with deuterium labelling studies. Hydrogen atoms in blue represent environments which were replaced with deuterium in isotope labelling studies, and CO_2 is shown in red. For clarity, only one isomer is shown in all cases. In reaction pathway i, CO_2insertion is shown as a 1-step process; alternatively, it could proceed in 2 steps by hydride abstraction from Si to generate a formate anion and Si-based cation, followed by formate coordination to Si. In reaction pathway ii, [Mn] represents [Mn(dmpe)$_2$] with or without dissociation of one phosphine donor. (*a*) this reaction could proceed in one step via Si–O bond-forming 1,2-insertion, or alternatively in two steps via initial Si–C bond-forming 1,2-insertion followed by a Brook-rearrangement-like 1,2-silyl group shift.

Summary and Conclusions

This work describes the reactions of Si*H*-substituted silyl dihydride complexes [(dmpe)$_2$MnH$_2$(SiHR$_2$)] (**1^{R2}**) and [(dmpe)$_2$MnH$_2$(SiH$_2$R)] (**1^{R}**) with CO_2, a widely available and inexpensive C1 synthon, to prepare formate-substituted silyl dihydride complexes [(dmpe)$_2$MnH$_2${Si(κ^1-O$_2$CH)R$_2$}] (**2^{R2}**) and [(dmpe)$_2$MnH$_2${Si(κ^1-O$_2$CH)$_2$R}] (**3^{R}**) under mild conditions (room temperature, 1.1 atm. CO_2). Diaryl- or dialkyl-substituted silyl dihydride complexes **1^{R2}** reacted with a single equivalent of CO_2 within minutes to yield **2^{R2}**. By contrast, monosubstituted silyl dihydride precursors **1^{R}** reacted with two equivalents of CO_2 in a stepwise fashion; insertion into one terminal Si–H bond occurred rapidly to yield [(dmpe)$_2$MnH$_2${SiH(κ^1-O$_2$CH)R}] (**4^{R}**), with one formate group on silicon, while insertion of the second equivalent of CO_2 into the remaining terminal Si–H bond to yield **3^{R}** proceeded over the course of several days. In the syntheses of **3^{R}**, appreciable amounts of H_2 and the carbonyl formate complex *trans*-

[(dmpe)$_2$Mn(CO)(κ^1-O$_2$CH)] (**5**) were observed, likely formed via initial H_2 elimination from **4^{R}** and/or **3^{R}**. In solution, compounds **2^{R2}** and **3^{R}** were observed to exist as the silicate isomer, and compound **2^{Ph2}** also crystallized as the silicate isomer. However, DFT calculations on **2^{Ph2}**, **3^{Ph}** and **4^{Ph}** indicated the thermodynamic accessibility of *trans*-hydrosilane/hydride, *trans*-dihydrogen/silyl, and *lateral*-dihydrogen/silyl isomers (these isomers were 3–45 kJ mol^{-1} higher in energy than the most stable experimentally observed isomer, depending on the identity of the substituents), and revealed strengthening of the Mn–Si interactions (in all isomers) with increasing formate substitution on silicon.

Reaction of CO_2 with [(dmpe)$_2$MnD$_2$(SiH$_2$^{n}Bu)] (***d*$_2$-1^{Bu}**) formed ***d*$_2$-3^{Bu}** as the major reaction product, predominantly (>95%) as [(dmpe)$_2$MnD$_2${Si(κ^1-O$_2$CH)$_2$^{n}Bu}] featuring two deuteride ligands. This labelling experiment is consistent with a mechanism involving direct insertion of CO_2 into a terminal Si–H bond in the silicate isomer of ***d*$_2$-1^{Bu}**, which would bear similarity to previously reported reactions of CO_2 or ketones with transition metal η^3-H$_2$SiRH complexes or metal-free hypercoordinate hydrosilanes. However, a more traditional mechanism involving initial CO_2 coordination to manganese and ensuing metal-based reactivity is also plausible. Future work will focus on experimental and computational studies to gain further insight into the mechanism of this reactivity, and investigation of its potential for catalytic hydrosilylation of CO_2 (or alternative unsaturated substrates).

Declaration of Competing Interest

The authors declare no conflicts of interest.

Acknowledgements

D. J. H. E. thanks NSERC of Canada for a Discovery Grant and Compute Canada for a 2020 Resources for Research Groups (RRG) grant. We are also grateful to Maia Murphy for collecting variable temperature NMR data.

Experimental

General Methods. An argon-filled MBraun UNIlab glove box equipped with a –30 °C freezer was employed for the manipulation and storage of all oxygen- and moisture- sensitive compounds. Air-sensitive preparative reactions were performed on a double-manifold high-vacuum line equipped with a two stage Welch 1402 belt-drive vacuum pump (ultimate pressure 1 × 10^{-4} torr) using standard techniques.[35] The vacuum was measured periodically using a Kurt J. Lesker 275i convection enhanced Pirani gauge. Residual oxygen and moisture were removed from the argon stream by passage through an Oxisorb-W scrubber from Matheson Gas Products.

Benzene was purchased from Aldrich, hexanes and THF were purchased from Caledon, and deuterated solvents were purchased from ACP Chemicals. Benzene, hexanes, and THF were initially dried and distilled at atmospheric pressure from sodium/benzophenone. All solvents were stored over an appropriate drying agent (benzene, THF, C_6D_6, d_8-toluene = Na/Ph$_2$CO; hexanes = Na/Ph$_2$CO/tetraglyme) and introduced to reactions or solvent storage flasks via vacuum transfer with condensation at –78 °C.

Dmpe, H$_3$SiPh, H$_3$Si^{n}Bu, H$_2$SiEt$_2$, H$_2$SiPh$_2$, 1,4-dioxane, CO_2 (99.8 %), D_2 (99.96 %), and ethylmagnesium chloride solution (2.0 M in diethyl ether) were purchased from Sigma-Aldrich. Manganese dichloride was purchased from Strem Chemicals. Argon (99.999 %) and hydrogen gas (99.999 %) were purchased from PraxAir. [(dmpe)$_2$MnH$_2$(SiHPh$_2$)] (**1^{Ph2}**),[23] [(dmpe)$_2$MnH$_2$(SiHEt$_2$)] (**1^{Et2}**),[23]

[(dmpe)$_2$MnH$_2$(SiH$_2$Ph)] (**1^{Ph}**),[24] [(dmpe)$_2$MnH$_2$(SiH$_2$^{n}Bu)] (**1^{Bu}**),[24] and [(dmpe)$_2$MnD$_2$(SiH$_2$^{n}Bu)] (***d*$_2$-1^{Bu}**)[24] were prepared using literature procedures.

NMR spectroscopy was performed on Bruker AV-500 and AV-600 spectrometers. Spectra were obtained at 298 K unless otherwise indicated. All ^{1}H NMR spectra were referenced relative to SiMe$_4$ through a resonance of the protio impurity of the solvent used: C_6D_6 (δ 7.16 ppm) or d_8-toluene (δ 2.08 ppm, 6.97 ppm, 7.01 ppm, and 7.09 ppm). The ^{2}H NMR spectra were referenced relative to the solvent used {C_6D_6 (δ 7.16 ppm)}. Also, all ^{13}C NMR spectra were referenced relative to SiMe$_4$ through a resonance of the ^{13}C in the solvent: C_6D_6 (δ 128.06 ppm) or d_8-toluene (δ 20.43, 125.13, 127.96, 128.87, and 137.48 ppm). The ^{29}Si and ^{31}P NMR spectra were referenced using indirect referencing from a ^{1}H NMR spectrum.[36]

Combustion elemental analysis was performed by Midwest Microlabs in Indianapolis.

Single-crystal X-ray crystallographic analysis of **2^{Ph2}** was performed on a crystal coated in Paratone oil and mounted on a Bruker SMART APEX II diffractometer with a 3 kW sealed-tube Mo generator and APEX II CCD detector in the McMaster Analytical X-Ray (MAX) Diffraction Facility. A semi-empirical absorption correction was applied using redundant and symmetry related data. Raw data was processed using XPREP (as part of the APEX v2.2.0 software), and solved by intrinsic (SHELXT)[37] methods. The structure was completed by difference Fourier synthesis and refined with full-matrix least-squares procedures based on F^2. Non-hydrogen atoms were refined anisotropically and hydrogen atoms were generated in ideal positions and then updated with each cycle of refinement (with the exceptions of hydrogen atoms bridging between Si(1) and Mn(1), or on C(1), which were located from the difference map and refined isotropically). Refinement was performed with SHELXL[38] in Olex2.[39]

All calculated structures were fully optimized with the ADF DFT package (SCM, version 2017.207 or 2019.305).[40] Calculations were conducted in the gas phase within the generalized gradient approximation using the 1996 Perdew-Burke-Ernzerhof exchange and correlation functional (PBE),[41] using the scalar zeroth-order regular approximation (ZORA)[42] for relativistic effects, and Grimme's DFT-D3-BJ dispersion correction.[43] Geometry optimizations were conducted with all-electron triple-ζ basis sets with two polarization functions (TZ2P), fine integration grids (Becke[44] verygood-quality), and default convergence criteria for energy and gradients. Bond orders were calculated within the Mayer[45] formalism. Visualization of the computational results was performed using the ADF-GUI (SCM) or Biovia Discovery Studio Visualizer. Analytical frequency calculations[46] were conducted on all geometry optimized structures to ensure that the geometry optimization led to an energy minimum. All reported computational values in this work were derived from restricted calculations (for modeling diamagnetic structures). For each structure, up to 8 energy minima were located for different potential rotamers, and the reported energies correspond to the global minimum for each isomer.

All prepared complexes are air sensitive, and their products upon reaction with air are malodorous. Therefore, all syntheses were conducted under an atmosphere of argon or CO_2.

[(dmpe)$_2$MnH$_2${Si(*κ*^{1}-O$_2$CH)Ph$_2$}] (2^{Ph2}). 190.1 mg (0.35 mmol) of [(dmpe)$_2$MnH$_2$(SiHPh$_2$)] (**1^{Ph2}**) was dissolved in 20 mL of benzene. The reaction mixture was freeze/pump/thawed in a 100 mL storage flask three times, placed under 1 atm. of CO_2 at 0 °C, and then sealed. After stirring at room temperature for two hours, the solvent was removed *in vacuo* and the resulting solid was washed with toluene and extracted with THF, leaving behind some residual solid. The THF solution was layered with hexanes and allowed to sit at –30 °C for a week, yielding 83.6 mg of **2^{Ph2}** as a yellow solid. The aforementioned residual solid was dried *in vacuo* to yield an additional 38.1 mg of **2^{Ph2}**. Furthermore, an additional 9.3 mg of **2^{Ph2}**

was obtained by allowing the toluene washings to sit at –30 °C for a week, and finally an additional 4.0 mg of **2^{Ph2}** was obtained by concentrating the THF/hexanes mother liquors, re-layering with hexanes, and allowing to sit at –30 °C for a week, for a total yield of 135.0 mg (0.23 mmol; 66 %) of **2^{Ph2}** as an analytically pure yellow solid. X-ray quality crystals were grown by layering a concentrated solution of **2^{Ph2}** in THF with hexanes, and allowing to stand at –30 °C for a week. **^{1}H NMR** (d_8-toluene, 600 MHz, 298 K): δ 8.87 (s, 1H, κ^1-O$_2$C*H*), 8.18 (d, 2H, $^3J_{H,H}$ 7.1 Hz, *o*), 7.71 (d, 2H, $^3J_{H,H}$ 7.2 Hz, *o*), 7.32 (t, 2H, $^3J_{H,H}$ 7.4 Hz, *m*), 7.22 (t, 1H, $^3J_{H,H}$ 7.2 Hz, *p*), 7.08 (*m*),[47] 7.02 (*p*),[47] 1.48 (d, 6H, $^2J_{H,P}$ 5.0 Hz, PCH_3), 1.26, 0.93 (2 × m, 4H, PCH_2), 1.02 (d, 6H, $^2J_{H,P}$ 6.0 Hz, PCH_3), 0.81 (d, 6H, $^2J_{H,P}$ 2.8 Hz, PCH_3), 0.61 (d, 6H, $^2J_{H,P}$ 5.7 Hz, PCH_3), –13.46 (s, 2H, Mn*H*). **^{13}C{H} NMR** (d_8-toluene, 151 MHz, 298 K): δ 162.65 (s, κ^1-O$_2$*C*H), 151.36, 150.21 (2 × s, *i*), 136.18, 134.72 (2 × s, *o*), 127.73 (s, *p*), 127.44, 127.33 (2 × s, *m* and *p*), 127.13 (s, *m*), 35.54, 32.04 (2 × m, P*C*H$_2$), 29.34, 23.67, 21.05 (3 × m, P*C*H$_3$), 24.46 (d, $^2J_{H,P}$ 16.7 Hz, P*C*H$_3$). **^{29}Si NMR** (d_8-toluene, 99 MHz, 298 K): δ 39.3.[47] **^{31}P{H} NMR** (d_8-toluene, 243 MHz, 298 K): δ 69.64, 68.70 (2 × br. s, 2P). **Anal**. Found (calcd.): C, 51.59 (51.37); H, 8.14 (7.76).

[(dmpe)$_2$MnH$_2${Si(κ^1-O$_2$CH)Et$_2$}] (2^{Et2}). Approx. 10 mg of [(dmpe)$_2$MnH$_2$(SiHEt$_2$)] (**1^{Et2}**) was dissolved in approx. 0.6 mL of C_6D_6. The resulting solution was then placed in an NMR tube with a J-Young Teflon valve and was freeze-pump-thawed (x3). The NMR tube was then placed under an atmosphere of carbon dioxide at 0 °C, sealed, and allowed to sit for 45 minutes at room temperature. The resulting mixture was analyzed *in situ* without purification, with 100% conversion to **2^{Et2}** observed by NMR spectroscopy. ^{1}H NMR (C_6D_6, 500 MHz, 298 K): δ 8.72 (s, 1H, κ^1-O$_2$C*H*), 1.5-0.8 (m, 18H, PCH_2, SiCH_2CH$_3$ and SiCH$_2$CH_3), 1.32, 1.28, 1.21, 0.79 (4 × s, 6H, PCH_3), –13.82 (s, 2H, Mn*H*). **^{13}C{H} NMR** (C_6D_6, 126 MHz, 298 K): δ 162.45 (s, κ^1-O$_2$*C*H), 35.53, 31.90 (2 × m, P*C*H$_2$), 30.40 (app. t, $J_{H,P}$ 15.2 Hz, P*C*H$_3$), 26.37, 23.95, 22.24 (3 × m, PCH$_3$), 19.32, 19.08, 9.37, 8.85 (4 × s, Si*C*H$_2$CH$_3$ and SiCH$_2$*C*H$_3$). **^{29}Si NMR** (C_6D_6, 99 MHz, 298 K): δ 53.9.[47] **^{31}P{H} NMR** (C_6D_6, 202 MHz, 298 K): δ 71.99, 69.12 (2 × br. s, 2P).

[(dmpe)$_2$MnH$_2${Si(κ^1-O$_2$CH)$_2$Ph}] (3^{Ph}) and [(dmpe)$_2$MnH$_2${SiH(κ^1-O$_2$CH)Ph}] (4^{Ph}). Approx. 10 mg of [(dmpe)$_2$MnH$_2$(SiH$_2$Ph)] (**1^{Ph}**) was dissolved in approx. 0.6 mL of C_6D_6. The resulting solution was placed in an NMR tube with a J-Young Teflon valve and was freeze-pump-thawed (x3). The NMR tube was then placed under an atmosphere of carbon dioxide at 0 °C, sealed, and allowed to sit at room temperature. The resulting mixture was analyzed *in situ* without purification after sitting for ~15 minutes (to obtain data for intermediate **4^{Ph}**) or 2 weeks (to obtain data for **3^{Ph}**). After 15 minutes, 100% consumption of **1^{Ph}** was observed, yielding an 8 : 1 mixture of **4^{Ph}** and **3^{Ph}**. After 2 weeks, an approximate 1 : 5 : 2 mixture of **4^{Ph}**, **3^{Ph}** and [(dmpe)$_2$Mn(CO)(κ^1-O$_2$CH)] (**5**) was observed. *NMR data for **4^{Ph}**:* ^{1}H NMR (C_6D_6, 500 MHz, 298 K): δ 8.84 (s, 1H, κ^1-O$_2$C*H*), 8.24, 7.38, 7.24 (3 × s, *o*, *m*, and *p*), 6.86 (s with ^{19}Si sat., 1H, $^1J_{H,Si}$ 202 Hz, Si*H*), 1.31, 1.21, 1.11, 0.79 (4 × s, dmpe), –13.51 (s, 2H, Mn*H*). **^{29}Si NMR** (C_6D_6, 99 MHz, 298 K): δ 31.3.[47] **^{31}P{H} NMR** (C_6D_6, 202 MHz, 298 K): δ 72.14, 69.45 (2 × br. s, 2P). *NMR data for **3^{Ph}**:* ^{1}H NMR (C_6D_6, 500 MHz, 298 K): δ 8.78, 8.50 (2 × s, 1H, κ^1-O$_2$C*H*), 8.08 (d, 2H, $^3J_{H,H}$ 8.0 Hz, *o*), 7.27 (t, 2H, $^3J_{H,H}$ 7.4 Hz, *m*), 7.18 (t, 1H, $^3J_{H,H}$ 7.5 Hz, *p*), 1.27 (m, 6H, PCH_3),[48] 1.25, 1.18 (2 × m, 2H, PCH_2),[47] 1.11 (d, 6H, $^2J_{H,P}$ 6.5 Hz, PCH_3), 1.08 (d, 6H, $^2J_{H,P}$ 6.7 Hz, PCH_3), 0.94, 0.84 (2 × m, 2H, PCH_2), 0.70 (d, 6H, $^2J_{H,P}$ 2.6 Hz, PCH_3), –13.89 (s, 2H, MnH_2). **^{13}C{H} NMR** (C_6D_6, 126 MHz, 298 K): δ 161.78, 160.98 (2 × s, κ^1-O$_2$*C*H), 148.09 (s, *i*), 134.45 (s, *o*), 128.4 (*p*),[47] 127.8 (*m*),[47] 34.31, 31.74 (2 × m, P*C*H$_2$), 29.23, 22.81 (2 × m, PCH$_3$), 25.14 (d, $^2J_{H,P}$ 21.0 Hz, P*C*H$_3$), 21.21 (d, $^2J_{H,P}$ 19.9 Hz, P*C*H$_3$). **^{29}Si NMR** (C_6D_6, 99 MHz, 298 K): δ 34.2.[47] **^{31}P{H} NMR** (C_6D_6, 202 MHz, 298 K): δ 71.10, 68.24 (2 × br. s, 2P).

[(dmpe)$_2$MnH$_2${Si(κ^1-O$_2$CH)$_2$^{n}Bu}] (3^{Bu}) and [(dmpe)$_2$MnH$_2${SiH(κ^1-O$_2$CH)^{n}Bu}] (4^{Bu}). **3^{Bu}** and **4^{Bu}** were prepared in a manner analogous to **3^{Ph}** and **4^{Ph}**, using [(dmpe)$_2$MnH$_2$(SiH$_2$^{n}Bu)] (**1^{Bu}**) in place of **1^{Ph}**. The

resulting mixture was analyzed *in situ* without purification after sitting for ~30 minutes (to obtain data for intermediate **4^{Bu}**) or 5 days (to obtain data for **3^{Bu}**). After 30 minutes, 100% consumption of **1^{Bu}** was observed, yielding a 10 : 1 mixture of **4^{Bu}** and **3^{Bu}**, respectively. After 5 days, no more **4^{Bu}** remained, and an approximate 7.5 : 1 mixture of **3^{Bu}** and [(dmpe)$_2$Mn(CO)(κ^1-O$_2$CH)] (**5**) was observed. *NMR data for **4^{Bu}**:* ^{1}H NMR (C_6D_6, 500 MHz, 298 K): δ 8.74 (s, 1H, κ^1-O$_2$C*H*), 6.31 (s with ^{19}Si sat., 1H, $^1J_{H,Si}$ 190 Hz, Si*H*), 1.76, 1.58, 1.33, 1.26, 1.06, 0.79 (6 × br. s, dmpe and ^{n}Bu), –13.74 (s, 2H, MnH_2). *NMR data for **3^{Bu}**:* ^{1}H NMR (C_6D_6, 500 MHz, 298 K): δ 8.64, 8.63 (2 × s, 1H, κ^1-O$_2$C*H*), 1.64 (m, 2H, SiCH$_2$C*H*$_2$CH$_2$CH$_3$), 1.47 (quin., 2H, $^3J_{H,H}$ 6.8 Hz, SiCH$_2$CH$_2$C*H*$_2$CH$_3$), 1.30 (d, 6H, $^2J_{H,P}$ 4.7 Hz, PC*H*$_3$), 1.28, 1.11 (2 × 3H, PC*H*$_2$ and SiC*H*$_2$CH$_2$CH$_2$CH$_3$), 1.24 (br. S, 12H, PC*H*$_3$), 0.99 (t, 3H, $^3J_{H,H}$ 7.3 Hz, SiCH$_2$CH$_2$CH$_2$C*H*$_3$), 0.95, 0.87 (2 × m, 2H, PC*H*$_2$), 0.70 (s, 6H, PC*H*$_3$), –14.0 (s, 2H, Mn*H*). **^{13}C{H} NMR** (C_6D_6, 126 MHz, 298 K): δ 161.46, 160.89 (2 × s, κ^1-O$_2$*C*H), 34.64, 31.73 (2 × m, P*C*H$_2$), 31.00 (s, Si*C*H$_2$CH$_2$CH$_2$CH$_3$), 29.50, 25.57, 22.95, 21.78 (4 × m, P*C*H$_3$), 27.49 (s, SiCH$_2$*C*H$_2$CH$_2$CH$_3$), 26.62 (s, SiCH$_2$CH$_2$*C*H$_2$CH$_3$), 14.40 (s, SiCH$_2$CH$_2$CH$_2$*C*H$_3$). **^{29}Si NMR** (C_6D_6, 99 MHz, 298 K): δ 46.5.[47] **^{31}P{H} NMR** (C_6D_6, 202 MHz, 298 K): δ 72.46, 67.94 (2 × br. s, 2P).

[(dmpe)$_2$MnD$_2${Si(κ^1-O$_2$CH)$_2$^{n}Bu}] (*d*$_2$-3^{Bu}). Approx. 10 mg of [(dmpe)$_2$MnD$_2$(SiH$_2$^{n}Bu)] (***d*$_2$-1^{Bu}**) was dissolved in approx. 0.6 mL of C_6D_6. The resulting solution was then placed in an NMR tube with a J-Young Teflon valve and was freeze-pump-thawed (x3). The NMR tube was then placed under an atmosphere of carbon dioxide at 0 °C, sealed, and allowed to sit at room temperature for 2 days. The resulting mixture was analyzed by ^{1}H and ^{2}H NMR spectroscopy *in situ* without purification. Compound ***d*$_2$-3^{Bu}** was formed cleanly as the major reaction product, and based on integration of the hydride and formate regions, this product is predominantly (>95%) [(dmpe)$_2$MnD$_2${Si(κ^1-O$_2$CH)$_2$^{n}Bu}] featuring two deuteride ligands. A small formate signal was observed in the ^{2}H NMR spectrum, attributable to a deuterated formate group (O$_2$CD) within either ***d*$_2$-3^{Bu}** or ***d*$_1$-5**. A small amount of ***d*$_n$-5** (n = 0 and/or 1) was also observed in the ^{1}H NMR spectrum (~5% relative to ***d*$_2$-3^{Bu}** based on integration of a PC*H*$_2$ signal in ***d*$_n$-5** relative to signals for ***d*$_2$-3^{Bu}**). ^{1}H, ^{13}C, and ^{31}P NMR data for ***d*$_2$-3^{Bu}** matches that of **3^{Bu}**, but without the Mn*H* ^{1}H NMR environment. ^{2}H NMR (C_6D_6, 77 MHz, 298 K): δ –14.18 (s, Mn*D*).

Appendix A. Supplementary Data

CCDC # 2077422 contains the supplementary crystallographic data for **2^{Ph2}**. These data can be obtained free of charge via http://www.ccdc.cam.ac.uk/conts/retrieving.html, or from the Cambridge Crystallographic Data Centre, 12 Union Road, Cambridge CB2 1EZ, UK; fax: (+44) 1223-336-033; or e-mail: deposit@ccdc.cam.ac.uk. Supplementary data to this article can be found online. PDF: Tables and figures of computational results and crystallographic data, and selected NMR spectra. XYZ: Coordinates of calculated structures.

References

1. (a) Brook, M. A., Chapter 12.8: Hydrosilylation. In *Silicon in Organic, Organometallics, and Polymer Chemistry*, John Wiley & Sons: New York, 2000; pp 401-422; (b) Roy, A. K., A Review of Recent Progress in Catalyzed Homogeneous Hydrosilation (Hydrosilylation). *Adv. Organomet. Chem.* **2008,** *55*, 1-59; (c) Marciniec, B.; Maciejewski, H.; Pietraszuk, C.; Pawluć, P., *Hydrosilylation: A Comprehensive Review on Recent Advances*. Springer: Netherlands, 2009; Vol. 1.
2. (a) Sakakura, T.; Choi, J.-C.; Yasuda, H., Transformation of Carbon Dioxide. *Chem. Rev.* **2007,** *107* (6), 2365-2387; (b) Cokoja, M.; Bruckmeier, C.; Rieger, B.; Herrmann, W. A.; Kühn, F. E., Transformation of Carbon Dioxide with Homogeneous Transition-Metal Catalysts: A Molecular Solution to a Global Challenge? *Angew. Chem., Int. Ed.* **2011,** *50* (37), 8510-8537; (c) Omae, I., Recent developments in carbon

dioxide utilization for the production of organic chemicals. *Coord. Chem. Rev.* **2012,** *256* (13-14), 1384-1405; (d) Hölscher, M.; Guertler, C.; Keim, W.; Müller, T. E.; Peters, M.; Leitner, W., Carbon Dioxide as a Carbon Resource – Recent Trends and Perspectives. *Z. Naturforsch., B: J. Chem. Sci.* **2012,** *67* (10), 961-975; (e) Aresta, M.; Dibenedetto, A.; Quaranta, E., State of the art and perspectives in catalytic processes for CO_2 conversion into chemicals and fuels: The distinctive contribution of chemical catalysis and biotechnology. *J. Catal.* **2016,** *343*, 2-45; (f) Li, Y.; Cui, X.; Dong, K.; Junge, K.; Beller, M., Utilization of CO_2 as a C1 Building Block for Catalytic Methylation Reactions. *ACS Catal.* **2017,** *7* (2), 1077-1086.

3. Luo, Y.-R., Bond Dissociation Energies. In *CRC Handbook of Chemistry and Physics*, 90 ed.; Lide, D., Ed. CRC Press 2010.

4. Chalk, A. J.; Harrod, J. F., Homogeneous Catalysis. II. The Mechanism of the Hydrosilation of Olefins Catalyzed by Group VIII Metal Complexes. *J. Am. Chem. Soc.* **1965,** *87* (1), 16-21.

5. Schroeder, M. A.; Wrighton, M. S., Pentacarbonyliron(0) Photocatalyzed Reactions of Trialkylsilanes with Alkenes. *J. Organomet. Chem.* **1977,** *128* (3), 345-58.

6. (a) Ojima, I.; Nihonyanagi, M.; Kogure, T.; Kumagai, M.; Horiuchi, S.; Nakatsugawa, K., Reduction of Carbonyl Compounds via Hydrosilylation. I. Hydrosilylation of Carbonyl Compounds Catalyzed by Tris(triphenylphosphine)chlororhodium. *J. Organomet. Chem.* **1975,** *94* (3), 449-61; (b) Ojima, I.; Kogure, T.; Kumagai, M.; Horiuchi, S.; Sato, T., Reduction of Carbonyl Compounds via Hydrosilylation. II. Asymmetric Reduction of Ketones via Hydrosilylation Catalyzed by a Rhodium(I) Complex with Chiral Phosphine Ligands. *J. Organomet. Chem.* **1976,** *122* (1), 83-97.

7. Zheng, G. Z.; Chan, T. H., Regiocontrolled Hydrosilation of *α,β*-Unsaturated Carbonyl Compounds Catalyzed by Hydridotetrakis(triphenylphosphine)rhodium(I). *Organometallics* **1995,** *14* (1), 70-9.

8. Lipke, M. C.; Liberman-Martin, A. L.; Tilley, T. D., Electrophilic Activation of Silicon–Hydrogen Bonds in Catalytic Hydrosilations. *Angew. Chem., Int. Ed.* **2017,** *56* (9), 2260-2294.

9. Lipke, M. C.; Tilley, T. D., Hypercoordinate Ketone Adducts of Electrophilic η^3-H_2SiRR' Ligands on Ruthenium as Key Intermediates for Efficient and Robust Catalytic Hydrosilation. *J. Am. Chem. Soc.* **2014,** *136* (46), 16387-16398.

10. Glaser, P. B.; Tilley, T. D., Catalytic Hydrosilylation of Alkenes by a Ruthenium Silylene Complex. Evidence for a New Hydrosilylation Mechanism. *J. Am. Chem. Soc.* **2003,** *125* (45), 13640-13641.

11. (a) Lipke, M. C.; Poradowski, M.-N.; Raynaud, C.; Eisenstein, O.; Tilley, T. D., Catalytic Olefin Hydrosilations Mediated by Ruthenium η^3-H_2Si σ Complexes of Primary and Secondary Silanes. *ACS Catal.* **2018,** *8* (12), 11513-11523; (b) Smith, P. W.; Dong, Y.; Tilley, T. D., Efficient and selective alkene hydrosilation promoted by weak, double Si–H activation at an iron center. *Chem. Sci.* **2020,** *11* (27), 7070-7075.

12. (a) Watanabe, T.; Hashimoto, H.; Tobita, H., Hydrido(hydrosilylene)tungsten Complexes with Strong Interactions between the Silylene and Hydrido Ligands. *Angew. Chem., Int. Ed.* **2004,** *43* (2), 218-221; (b) Zhang, X.-H.; Chung, L. W.; Lin, Z.; Wu, Y.-D., A DFT Study on the Mechanism of Hydrosilylation of Unsaturated Compounds with Neutral Hydrido(hydrosilylene)tungsten Complex. *J. Org. Chem.* **2008,** *73* (3), 820-829; (c) Watanabe, T.; Hashimoto, H.; Tobita, H., Hydrido(hydrosilylene)tungsten Complexes: Dynamic Behavior and Reactivity Toward Acetone. *Chem. - Asian J.* **2012,** *7* (6), 1408-1416.

13. Calimano, E.; Tilley, T. D., Reactions of Cationic PNP-Supported Iridium Silylene Complexes with Polar Organic Substrates. *Organometallics* **2010,** *29* (7), 1680-1692.

14. (a) Rendler, S.; Oestreich, M., Hypervalent Silicon as a Reactive Site in Selective Bond-Forming Processes. *Synthesis* **2005,** (11), 1727-1747; (b) Kraushaar, K.; Schmidt, D.; Schwarzer, A.; Kroke, E., Reactions of CO_2 and CO_2 Analogs (CXY with X, Y=O, S, NR) with Reagents Containing Si–H and Si–N Units. In *Advances in Inorganic Chemistry*, Aresta, M.; Eldik, R. V., Eds. 2014; Vol. 66, pp 117-162.

15. (a) Boyer, J.; Breliere, C.; Corriu, R. J. P.; Kpoton, A.; Poirier, M.; Royo, G., Enhancement of Silicon–Hydrogen Bond Reactivity in Pentacoordinated Structures. *J. Organomet. Chem.* **1986,** *311* (3), C39-C43; (b) Arya, P.; Boyer, J.; Corriu, R. J. P.; Lanneau, G. F.; Perrot, M., Reactivity of hypervalent species of silicon:

reduction of CO_2 to formaldehyde with formation of silanone. *J. Organomet. Chem.* **1988,** *346* (1), C11-C14.
16. von Wolff, N.; Lefèvre, G.; Berthet, J. C.; Thuéry, P.; Cantat, T., Implications of CO_2 Activation by Frustrated Lewis Pairs in the Catalytic Hydroboration of CO_2: A View Using N/Si^+ Frustrated Lewis Pairs. *ACS Catal.* **2016,** *6* (7), 4526-4535.
17. Ishida, S.; Hatakeyama, T.; Nomura, T.; Matsumoto, M.; Yoshimura, K.; Kyushin, S.; Iwamoto, T., A Six-Coordinate Silicon Dihydride Embedded in a Porphyrin: Enhanced Hydride-Donor Properties and the Catalyst-Free Hydrosilylation of CO_2. *Chem. - Eur. J.* **2020,** *26* (68), 15811-15815.
18. Weinmann, M.; Walter, O.; Huttner, G.; Lang, H., Reaction studies on hypervalent silicon hydride compounds. *J. Organomet. Chem.* **1998,** *561* (1-2), 131-141.
19. (a) Novák, M.; Dostál, L.; Alonso, M.; De Proft, F.; Růžička, A.; Lyčka, A.; Jambor, R., Hydrosilylation Induced by N→Si Intramolecular Coordination: Spontaneous Transformation of Organosilane into 1-Aza-Silole-Type Molecules in the Absence of a Catalyst. *Chem. - Eur. J.* **2014,** *20* (9), 2542-2550; (b) Novák, M.; Dostál, L.; Turek, J.; Alonso, M.; De Proft, F.; Růžička, A.; Jambor, R., Spontaneous Double Hydrometallation Induced by N→M Coordination in Organometallic Hydrides of Group 14 Elements. *Chem. - Eur. J.* **2016,** *22* (16), 5620-5628; (c) Witteman, L.; Evers, T.; Shu, Z.; Lutz, M.; Klein Gebbink, R. J. M.; Moret, M.-E., Hydrosilylation in Aryliminopyrrolide-Substituted Silanes. *Chem. - Eur. J.* **2016,** *22* (17), 6087-6099; (d) Novák, M.; Hošnová, H.; Dostál, L.; Glowacki, B.; Jurkschat, K.; Lyčka, A.; Ruzickova, Z.; Jambor, R., Hydrosilylation of RN=CH Imino-Substituted Pyridines without a Catalyst. *Chem. - Eur. J.* **2017,** *23* (13), 3074-3083; (e) Růžičková, Z.; Jambor, R.; Novák, M., Spontaneous Hydrosilylation of Substituted C=N Imines. *Eur. J. Inorg. Chem.* **2019,** *2019* (28), 3335-3342.
20. Luo, X. L.; Schulte, G. K.; Demou, P.; Crabtree, R. H., Unusual Stereochemical Rigidity in Seven-Coordination. Synthesis and Structural Characterization of $ReH_2(EPh_3)(CO)(PMe_2Ph)_3$ (E = Si, Sn). *Inorg. Chem.* **1990,** *29* (21), 4268-73.
21. Jagirdar, B. R.; Palmer, R.; Klabunde, K. J.; Radonovich, L. J., Metal Hydride vs Side-on *σ*-Bonded Trichlorosilane Complexes of Arene–Chromium Derivatives: (η^6-arene)$Cr(CO)(H)_2(SiCl_3)_2$. *Inorg. Chem.* **1995,** *34* (1), 278-83.
22. Zuzek, A. A.; Parkin, G., Si–H and Si–C Bond Cleavage Reactions of Silane and Phenylsilanes with $Mo(PMe_3)_6$: Silyl, Hypervalent Silyl, Silane, and Disilane Complexes. *J. Am. Chem. Soc.* **2014,** *136* (23), 8177-8180.
23. Price, J. S.; Emslie, D. J. H.; Britten, J. F., Manganese Silylene Hydride Complexes: Synthesis and Reactivity with Ethylene to Afford Silene Hydride Complexes. *Angew. Chem., Int. Ed.* **2017,** *56* (22), 6223-6227.
24. Price, J. S.; Emslie, D. J. H.; Berno, B., Manganese Silyl Dihydride Complexes: A Spectroscopic, Crystallographic, and Computational Study of Nonclassical Silicate and Hydrosilane Hydride Isomers. *Organometallics* **2019,** *38* (11), 2347-2362.
25. Gutsulyak, D. V.; Kuzmina, L. G.; Howard, J. A. K.; Vyboishchikov, S. F.; Nikonov, G. I., $Cp(Pr^{i2}MeP)FeH_2SiR_3$: Nonclassical Iron Silyl Dihydride. *J. Am. Chem. Soc.* **2008,** *130* (12), 3732-3733.
26. (a) Hussein, K.; Marsden, C. J.; Barthelat, J.-C.; Rodriguez, V.; Conejero, S.; Sabo-Etienne, S.; Donnadieu, B.; Chaudret, B., X-Ray structure and theoretical studies of $RuH_2(\eta^2\text{-}H_2)(\eta^2\text{-}H\text{-}SiPh_3)(PCy_3)_2$, a complex with two different η^2-coordinated σ bonds. *Chem. Commun.* **1999,** (14), 1315-1316; (b) Lachaize, S.; Sabo-Etienne, S.; Donnadieu, B.; Chaudret, B., Mechanistic studies on ethylene silylation with chlorosilanes catalyzed by ruthenium complexes. *Chem. Commun.* **2003,** (2), 214-215; (c) Osipov, A. L.; Gerdov, S. M.; Kuzmina, L. G.; Howard, J. A. K.; Nikonov, G. I., Syntheses and X-ray Diffraction Studies of Half-Sandwich Hydridosilyl Complexes of Ruthenium. *Organometallics* **2005,** *24* (4), 587-602; (d) Lee, T. Y.; Dang, L.; Zhou, Z.; Yeung, C. H.; Lin, Z.; Lau, C. P., Nonclassical Ruthenium Silyl Dihydride Complexes $TpRu(PPh_3)(\eta^3\text{-}HSiR_3H)$ [Tp = Hydridotris(pyrazolyl)borate]: Catalytic Hydrolytic Oxidation of Organosilanes to Silanols with $TpRu(PPh_3)(\eta^3\text{-}HSiR_3H)$. *Eur. J. Inorg. Chem.* **2010,** (36), 5675-5684; (e) Liu,

H.-J.; Landis, C.; Raynaud, C.; Eisenstein, O.; Tilley, T. D., Donor-Promoted 1,2-Hydrogen Migration from Silicon to a Saturated Ruthenium Center and Access to Silaoxiranyl and Silaiminyl Complexes. *J. Am. Chem. Soc.* **2015,** *137* (28), 9186-9194; (f) Mai, V. H.; Kuzmina, L. G.; Churakov, A. V.; Korobkov, I.; Howard, J. A. K.; Nikonov, G. I., NHC carbene supported half-sandwich hydridosilyl complexes of ruthenium: the impact of supporting ligands on Si···H interligand interactions. *Dalton Trans.* **2016,** *45* (1), 208-215.

27. Mautz, J.; Heinze, K.; Wadepohl, H.; Huttner, G., Reductive Activation of *tripod* Metal Compounds: Identification of Intermediates and Preparative Application. *Eur. J. Inorg. Chem.* **2008,** (9), 1413-1422.

28. Fasulo, M. E.; Calimano, E.; Buchanan, J. M.; Tilley, T. D., Multiple Si–H Bond Activations by $^{t}Bu_2PCH_2CH_2P^{t}Bu_2$ and $^{t}Bu_2PCH_2P^{t}Bu_2$ Di(phosphine) Complexes of Rhodium and Iridium. *Organometallics* **2013,** *32* (4), 1016-1028.

29. Wu, X.; Ding, G.; Lu, W.; Yang, L.; Wang, J.; Zhang, Y.; Xie, X.; Zhang, Z., Nickel-Catalyzed Hydrosilylation of Terminal Alkenes with Primary Silanes via Electrophilic Silicon–Hydrogen Bond Activation. *Org. Lett.* **2021,** *23* (4), 1434-1439.

30. Price, J. S.; Emslie, D. J. H., Interconversion and reactivity of manganese silyl, silylene, and silene complexes. *Chem. Sci.* **2019,** *10* (47), 10853-10869.

31. Price, J. S.; Emslie, D. J. H., Reactions of Manganese Silyl and Silylene Complexes with CO_2 and $C(N^{i}Pr)_2$: Synthesis of Mn(I) Formate and Amidinylsilyl Complexes. *Organometallics* **2020,** *39* (24), 4618-4628.

32. A related mechanism involving the *trans*-hydrosilane/hydride isomer of $\boldsymbol{d_2}$-**1**$^{\mathbf{Bu}}$ or $\boldsymbol{d_2}$-**4**$^{\mathbf{Bu}}$ is also conceivable.

33. Hydride abstraction from Si by CO_2 to initially generate a formate anion and a $[(dmpe)_2Mn(\eta^3\text{-}H_2SiRR']^+$ cation, followed by formate coordination to Si, is also conceivable.

34. A Mn–C(O)OSiHRR' linkage could be formed in one step, via Si–O bond-forming 1,2-insertion, or in two steps by initial Si–C bond forming 1,2-insertion to form a silyl carboxylate compound, $L_xMn(O_2CSiHRR')$, followed by a 1,2-silyl shift with resemblance to a Brook rearrangement.

35. B. J. Burger, J. E. B., Vacuum Line Techniques for Handling Air-Sensitive Organometallic Compounds. In *Experimental Organometallic Chemistry - A Practicum in Synthesis and Characterization*, American Chemical Society: Washington, D.C., 1987; Vol. 357, pp 79-98.

36. Harris, R. K.; Becker, E. D.; Cabral de Menezes, S. M.; Goodfellow, R.; Granger, P., NMR Nomenclature. Nuclear Spin Properties and Conventions for Chemical Shifts (IUPAC Recommendations 2001). *Pure Appl. Chem.* **2001,** *73* (11), 1795-1818.

37. Sheldrick, G. M., SHELXT - Integrated space-group and crystal-structure determination. *Acta Crystallogr., Sect. A: Found. Adv.* **2015,** *71* (1), 3-8.

38. Sheldrick, G. M., Crystal structure refinement with SHELXL. *Acta Crystallogr., Sect. C: Struct. Chem.* **2015,** *71* (1), 3-8.

39. Dolomanov, O. V.; Bourhis, L. J.; Gildea, R. J.; Howard, J. A. K.; Puschmann, H., OLEX2: a complete structure solution, refinement and analysis program. *J. Appl. Crystallogr.* **2009,** *42* (2), 339-341.

40. (a) ADF2010, SCM, Theoretical Chemistry, Vrije Universiteit, Amsterdam, The Netherlands, http://www.scm.com; (b) Guerra, C. F.; Snijders, J. G.; te Velde, G.; Baerends, E. J., Towards an order-*N* DFT method. *Theor. Chem. Acc.* **1998,** *99* (6), 391-403; (c) te Velde, G.; Bickelhaupt, F. M.; Baerends, E. J.; Fonseca Guerra, C.; Van Gisbergen, S. J. A.; Snijders, J. G.; Ziegler, T., Chemistry with ADF. *J. Comput. Chem.* **2001,** *22* (9), 931-967.

41. Perdew, J. P.; Burke, K.; Ernzerhof, M., Generalized Gradient Approximation Made Simple. *Phys. Rev. Lett.* **1996,** *77* (18), 3865-3868.

42. (a) van Lenthe, E.; Baerends, E. J.; Snijders, J. G., Relativistic regular two-component Hamiltonians. *J. Chem. Phys.* **1993,** *99* (6), 4597-610; (b) van Lenthe, E.; Baerends, E. J.; Snijders, J. G., Relativistic total energy using regular approximations. *J. Chem. Phys.* **1994,** *101* (11), 9783-92; (c) van Lenthe, E.; Snijders, J. G.; Baerends, E. J., The zero-order regular approximation for relativistic effects: The effect of spin-orbit

coupling in closed shell molecules. *J. Chem. Phys.* **1996,** *105* (15), 6505-6516; (d) van Lenthe, E.; van Leeuwen, R.; Baerends, E. J.; Snijders, J. G., Relativistic Regular Two-Component Hamiltonians. *Int. J. Quantum Chem.* **1996,** *57* (3), 281-93; (e) van Lenthe, E.; Ehlers, A.; Baerends, E. J., Geometry optimizations in the zero order regular approximation for relativistic effects. *J. Chem. Phys.* **1999,** *110* (18), 8943-8953.

43. (a) Grimme, S.; Antony, J.; Ehrlich, S.; Krieg, H., A consistent and accurate ab initio parametrization of density functional dispersion correction (DFT-D) for the 94 elements H-Pu. *J. Chem. Phys.* **2010,** *132* (15), 154104; (b) Grimme, S.; Ehrlich, S.; Goerigk, L., Effect of the Damping Function in Dispersion Corrected Density Functional Theory. *J. Comput. Chem.* **2011,** *32* (7), 1456-1465.

44. (a) Becke, A. D., A multicenter numerical integration scheme for polyatomic molecules. *J. Chem. Phys.* **1988,** *88* (4), 2547-2553; (b) Franchini, M.; Philipsen, P. H. T.; Visscher, L., The Becke Fuzzy Cells Integration Scheme in the Amsterdam Density Functional Program Suite. *J. Comput. Chem.* **2013,** *34* (21), 1819-1827.

45. (a) Mayer, I., Charge, Bond Order and Valence in the Ab Initio SCF Theory. *Chem. Phys. Lett.* **1983,** *97* (3), 270-4; (b) Mayer, I., Charge, Bond Order and Valence in the Ab Initio SCF Theory (Addendum). *Chem. Phys. Lett.* **1985,** *117* (4), 396; (c) Mayer, I., On Bond Orders and Valences in the *Ab Initio* Quantum Chemical Theory. *Int. J. Quantum Chem.* **1986,** *29* (1), 73-84; (d) Sannigrahi, A. B.; Kar, T., Three-center bond index. *Chem. Phys. Lett.* **1990,** *173* (5-6), 569-72; (e) Bridgeman, A. J.; Cavigliasso, G.; Ireland, L. R.; Rothery, J., The Mayer bond order as a tool in inorganic chemistry. *J. Chem. Soc., Dalton Trans.* **2001,** (14), 2095-2108.

46. (a) Bérces, A.; Dickson, R. M.; Fan, L.; Jacobsen, H.; Swerhone, D.; Ziegler, T., An implementation of the coupled perturbed Kohn-Sham equations: perturbation due to nuclear displacements. *Comput. Phys. Commun.* **1997,** *100* (3), 247-262; (b) Jacobsen, H.; Bérces, A.; Swerhone, D. P.; Ziegler, T., Analytic second derivatives of molecular energies: a density functional implementation. *Comput. Phys. Commun.* **1997,** *100* (3), 263-276; (c) Wolff, S. K., Analytical Second Derivatives in the Amsterdam Density Functional Package. *Int. J. Quantum Chem.* **2005,** *104* (5), 645-659.

47. Chemical shift located from a crosspeak in 2D NMR.

48. Chemical shift located from the $^{1}H\{^{31}P\}$ NMR spectrum.